ORIGINAL ARTICLE

lajss.org Latin American Journal of Solids and Structures

www.lajss.org

Experimental Studies on Shear Resistance Performances for the Shear key of H Shape Steel Spatial Grid Roofs

Hongkun Shang[a,b]

Kejian Ma[a*]

Yanhui Wei[a]

Yaqin Lu[a]

[a] Space Structures Research Center (SSRC), Guizhou University, China. E-mail: shanghongkun1981@sina.com, 33752987@qq.com, yhwei@gzu.edu.cn, luya_2000@163.com

[b] College of Civil Engineering, Qingdao University of Technology, China.

*Correspondence

http://dx.doi.org/10.1590/1679-78255571

Abstract

In this paper, a new type of structure was introduced. The spatial steel grid structure was composed of the top layer, lower layer H-shaped steel ribs and square steel tubes. The shear key is the key part of the structure.Based on the real dimensions of a practical prototype,two sets of full-scale shear key specimens were made, one of which has vertical stiffening ribs. The loading tests of two groups of specimens were carried out to simulate cases under pure shears and the experimental results were compared with the simulations from the finite element analysis. The effects of vertical stiffeners on failure modes, ultimate loads, strength-yield ratio and ductility of shear key were studied through experiments. By parametric analyses in the present article, relations of the stiffening plates width and thickness was recommended.

Keywords

Shear key; H shape steel; Shearing rigidity; Stiffeners; Ductility factor.

1. Introduction

With the decreases of cultivated lands and the shortage of urban lands, the demands for large-span and multi-storey buildings with small constructional depths are dramatically increasing. The selected constructional depth of a floor may

Received: March 31, 2019. In Revised Form: April 15, 2019. Accepted: April 23, 2019. Available online: April 24, 2019
http://dx.doi.org/10.1590/1679-78255571

CC BY

significantly affect the overall height of the building (De Silva & Thambiratnam 2009; Da Silva et al. 2003; El-Dardiry & Ji 2005). It is a trend for building structures to reduce the floor height by adopting new floor structures. The depth of beams increases with the increase of the span, which makes the beam deeper and heavier than expected for traditional floor structures. The long-span space steel grid structure is alternative in order to solve such problems. This type of structures provides appealing benefits in terms of construction costs such as large spanning capabilities with minimal materials, small floor heights, fast constructions, and the advantages offered by ordinary composite beam constructions (Lawson et al. 1999; Lawson et al. 2006; Hicks. 2003).

The long-span space steel grid structure is suitable for multi-storey, high-rise and long-span industrial and public buildings. It has been applied in many projects (Shang et al. 2018b) (Fig. 1). It is composed of orthogonal and orthogonal-diagonal lattice hollow grid plates which consist of steel hollow beams. The top and bottom ribs of the steel grid are made of profiled steel, and the middle is connected by square steel tube (Ma et al. 2006). The reinforced concrete floor slabs are poured on site (Fig. 2 and Fig.3). The mechanical model of the structure is a spatial plate, which has three-dimensional mechanical behaviors. As the steel grid is open, the structure has the characteristics of light weight, large stiffness and good human comfortness. Various pipelines are able to pass through the hollows of the steel grids which saves building space and reduces the cost of the project (Shang et al. 2018a). The shear key connect the top and bottom ribs of the structure, which makes the whole structure work together. The height and width of the shear key is exactly the same. The characteristic of the shear key determines the performance of the structure. However, few studies have been conducted on the failure mechanism and shear behavior of shear key as the core component of the structure. To date, investigations mainly focus on the static and dynamic analyses of the whole structure (Zhang & Ma 2003; Zhang et al. 2004; Zhang, 2010; Jiang & Zhang 2014; Bai et al. 2016; Cai et al. 2017).

The shear key is studied in this paper by the combination of theoretical analyses and experimental researches. The emphasis of the study is on shear behaviors under pure shear conditions. The investigations can provide technical supports for the engineering application, and have important theoretical and practical significance.



Fig.1 Engineering examples

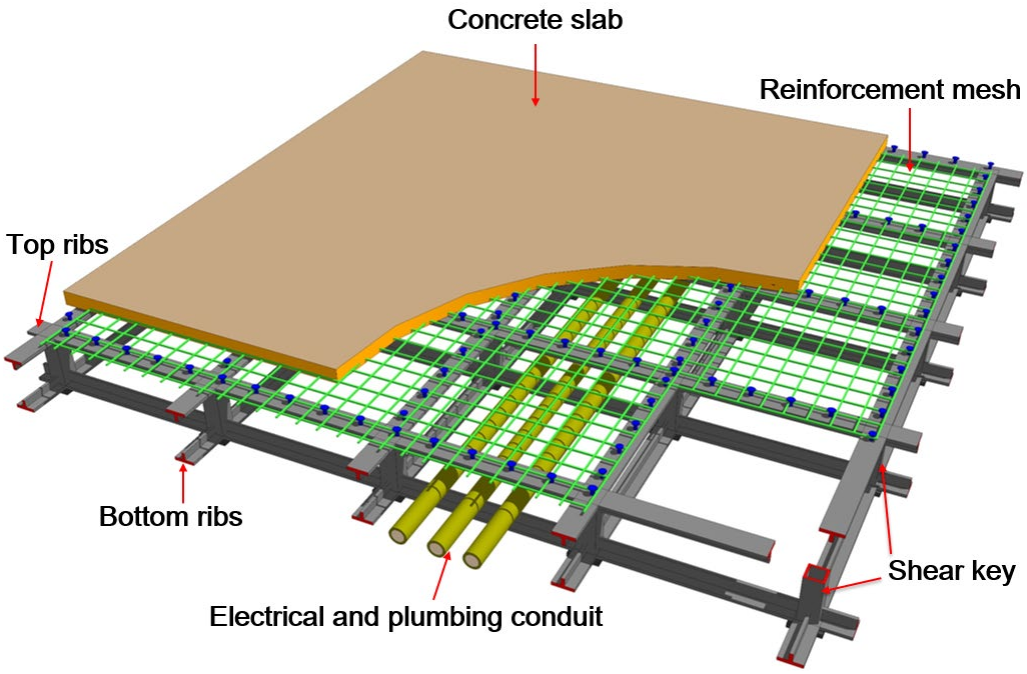

Fig.2 Components of the spatial steel grid structure

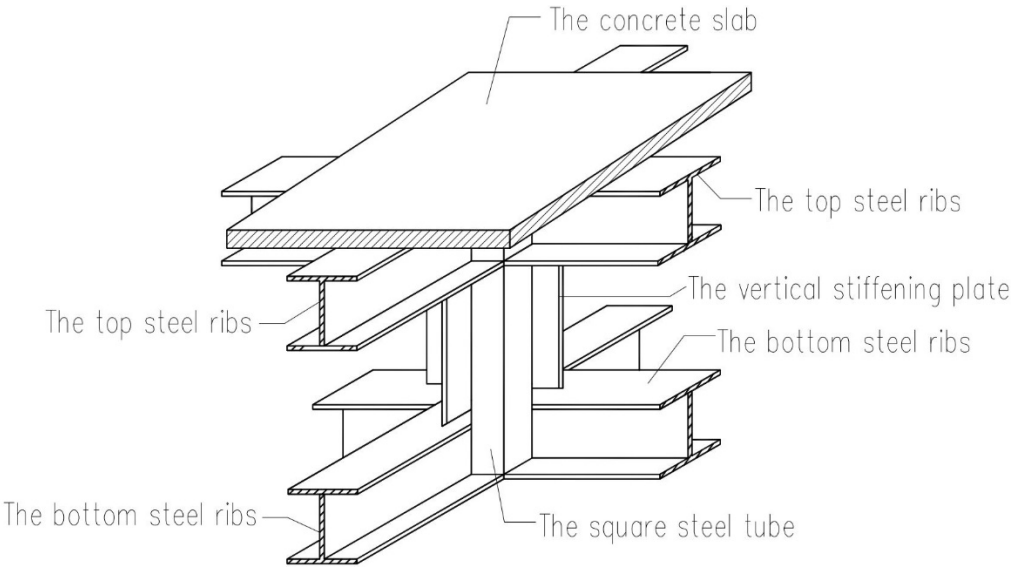

Fig.3 Components of shear key

2. Experimental Analysis

2.1 Test Specimens

This experiment is based on a practical project of a steel grid hospital building; two sets of full-scale shear key model are designed according to the sizes of the building. Each group contains two specimens, a total of four specimens.

To study the effect of vertical stiffening plate, one group of specimens is equipped with vertical stiffening plate, while the other group is not. The other conditions are identical for the specimens. The number and size of the specimens are shown in Fig. 4 and Fig. 5. Specimens of Group A do not have vertical stiffening plates, including A1 and A2; Specimens of Group B have the vertical stiffening plate, including B1 and B2.

2.2 Material Properties

The material properties of tubes, H-section steels and steel plates were measured in this paper. All material grades were Q345 stipulated in GB 50018-2002. All the stiffeners were fabricated from the same batch of steel sheets. The dimensions of the tensile coupon were conformed to the GB/T 228.1-2010 standard. An electronic universal material testing machine was used to apply load and record readings. The mechanical properties of the steel are shown in Table 1.

Table 1 Measured steel tube mechanical properties

Material type	Yield strength	Ultimate strength	Modulus of elasticity
	f_y/MPa	f_u/MPa	E_s/MPa
HW150X150X7X10	424	529	$1.94x10^5$
□150x150x6	421	523	$1.92x10^5$
Steel plate(t=6mm)	460	531	$2.08x10^5$

2.3 Layout of measuring points

The strain measurement points were mainly located in the square steel tube and the ends plate, as shown in Fig. 4 and Fig. 5.

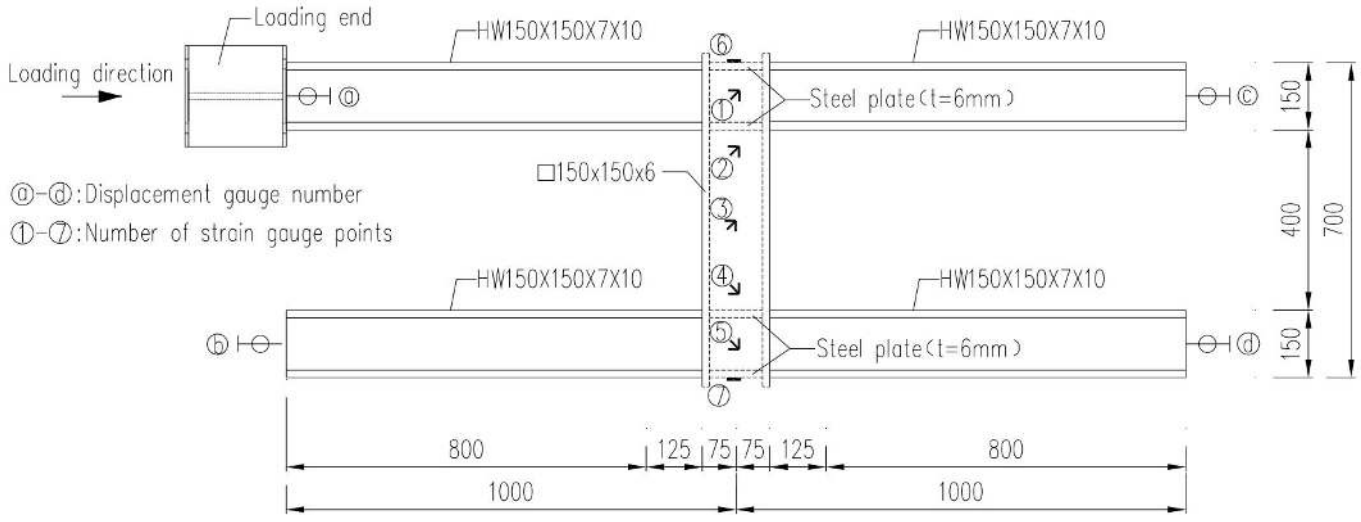

Fig.4 Dimensions of Group A and layout of measuring points

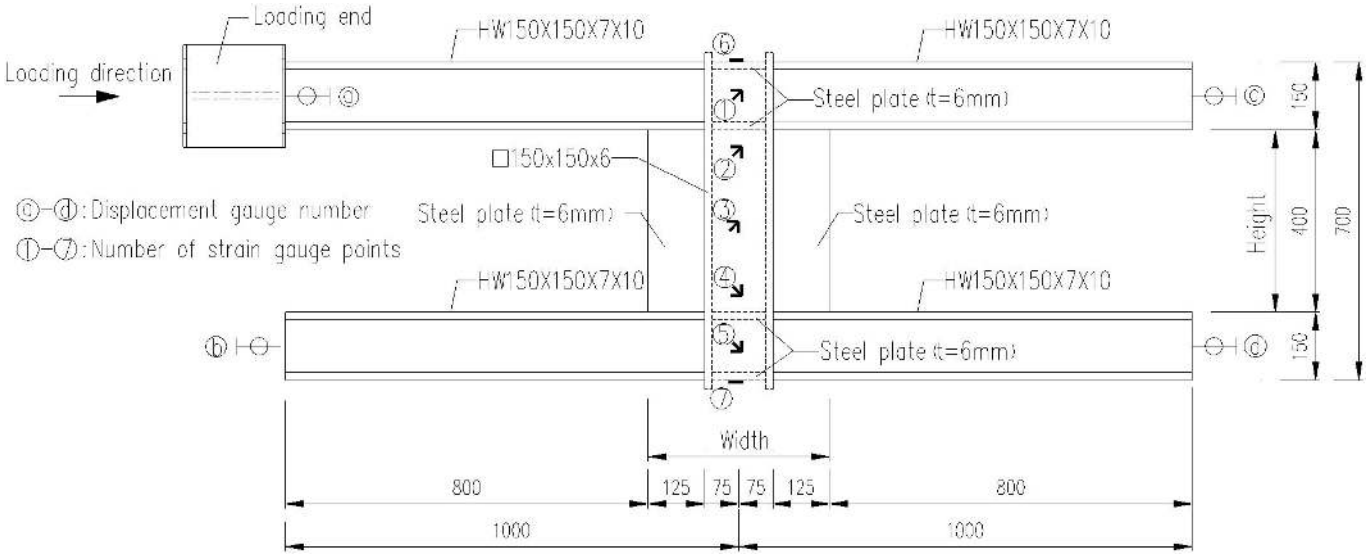

Fig.5 Dimensions of Group B and layout of measuring points

2.4 Test Setup and Procedure

The loading equipment was the electro-hydraulic servo loading system with a rated loading value of 1000kN. The strain acquisition equipment adopted TST3826F-L static strain testing and analysis system. The sensing equipment was JHBT-100T type load sensor. The displacement acquisition used one-dimensional displacement sensor.

The actuator was horizontally fixed on the reaction frame, and the specimens were fixed on the steel column with a special restraint device. In order to simulate the pure shear stress state, the hinged support was simulated by the steel bar passing through the circular hole of the lower rib; the other three ends of the ribs were constrained by the pulley support to ensure that the top and bottom ribs were able to slide along the horizontal direction. The loading diagram is shown in Fig. 6.

During the test, the specimens were loaded by stages at the interval of 10 minutes in order to observe the stress condition of the specimens. The specimen was initially loaded with 0.5kN to eliminate the relative displacement between the steel bar and the circular hole. Firstly, the ultimate load of the specimens was predicted according to theoretical analysis, and the load was graded by 1/20 of the ultimate load and slowly loaded. The displacement and strain at each stage of loading were recorded during the loading process. When the inflection point appears on the loading-displacement curves under local instability, the yield of the shear key was determined.

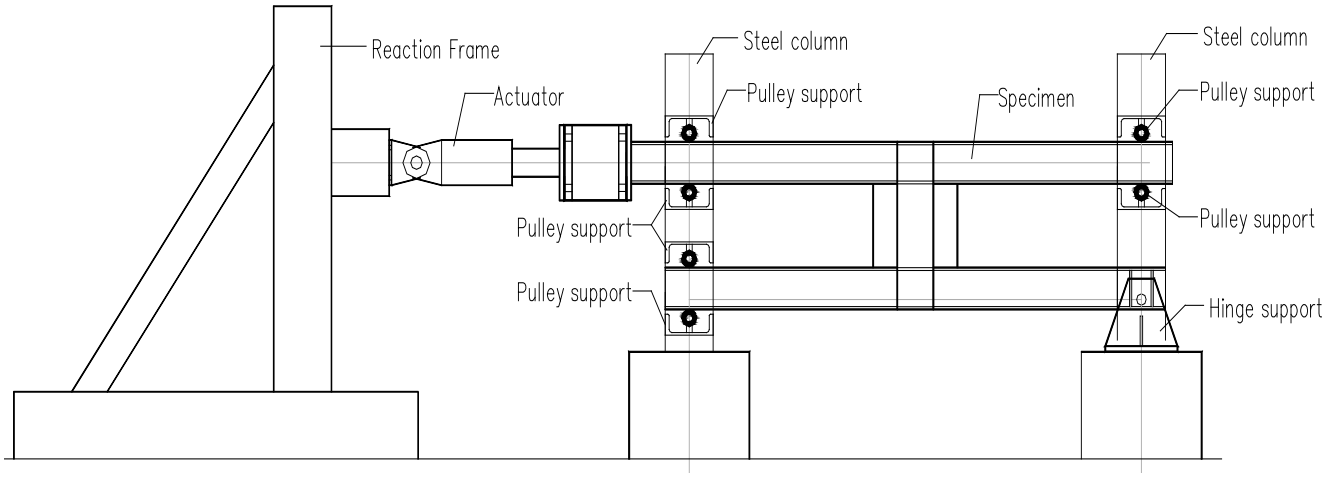

Fig.6 Schematic diagram of loading device

3. Test Results

3.1. Failure Mode

Specimens of group A(A-1 and A-2)showed elastic deformation characteristics at the initial stage of loading and the load showed a linear relationship with the displacement. When the load reached to 200KN, the connection area between square steel tube and rib began to enter the yield stage with the clacking. At the loading end, concave deformation began to appear on the upper part of square steel tube (Fig. 7a) with bulging deformation on the side (Fig. 7a) and the lower part of the tube was bulging (Fig. 7b). At the support end, convex deformation occurred on the upper part of the tube (Fig. 7c) and concave deformation occurred on the lower part (Fig. 7d). With the increase of the load, the desquamation phenomenon began to appear at the joint of square steel tube and ribs, and gradually expanded to both sides. By this time, the upper and lower end areas of tube had entered the plastic deformation stage while the displacement of the specimen increased rapidly and the strain develops rapidly. The middle of the specimen warped upward, the square steel tube inclined to the loading direction, and the tube presented the “Z” deformation (Fig. 8). When the load reached to 440KN, the deformation of the specimens increased rapidly with the clacking. The steel tube connecting the top and bottom ribs was torn and the test was completed. A-1 and A-2 specimens had similar experimental phenomena. The Integral deformation shape is shown in Fig. 8.

Specimens of group B showed elastic deformation characteristics at the initial stage of the loading and the load also showed a linear relationship with the displacement. When the load was close to 300KN, the bending deformation began to appear at the corner of the vertical stiffener (Fig. 9a and Fig. 9b). With the increase of the load, the bending deformation of vertical stiffeners increased. The flange of the top and bottom ribs began to bend (Fig. 9c and Fig. 9d). At this time, the flange of rib entered the stage of plastic deformation and the displacement of the specimen increased rapidly. When the load reached to 700KN, it was more than 15% of the theoretical ultimate load. The bending deformation of the top and bottom ribs occurred. The specimen emitted a “squeak” sound. The displacement of the specimen increased rapidly and the bearing capacity began to decrease. Then the test was terminated for safety reasons. At this time, there was no obvious deformation on the surface of the square steel tube. The shear key was intact as a whole and inclined slightly to the direction of loading. The stiffness of the shear key was enhanced because of the installation of vertical stiffeners. The bending deformation was dominant for the upper and lower ribs. B-1 and B-2 specimens exhibited similar experimental phenomena. The Integral deformation shape is shown in Fig. 10.

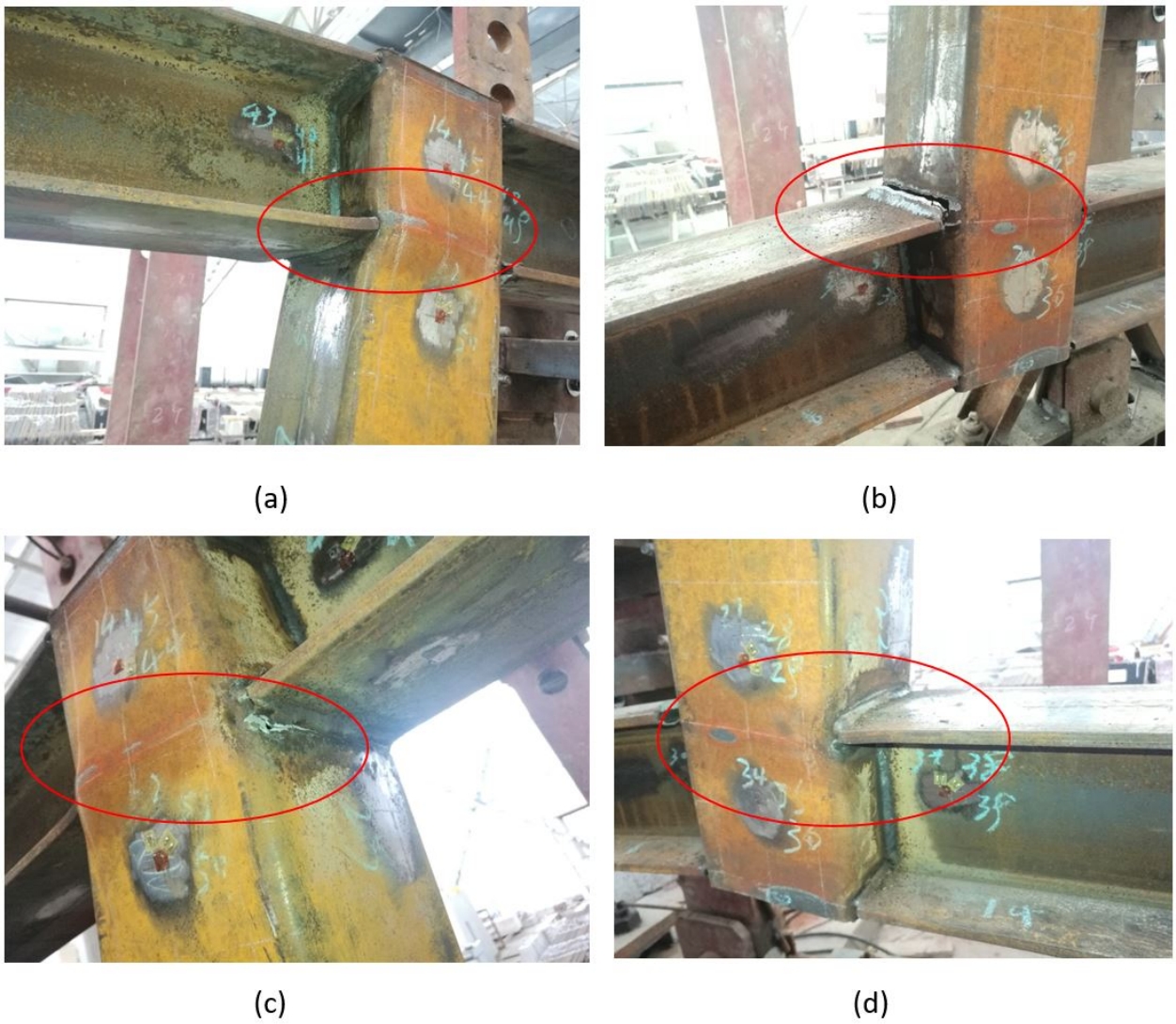

Fig.7 Detailed deformed shapes of A: (a) Deformation of the loading top; (b) Failure of the loading bottom; (c) Failure of the supporting top; (d) Deformation of the supporting bottom.

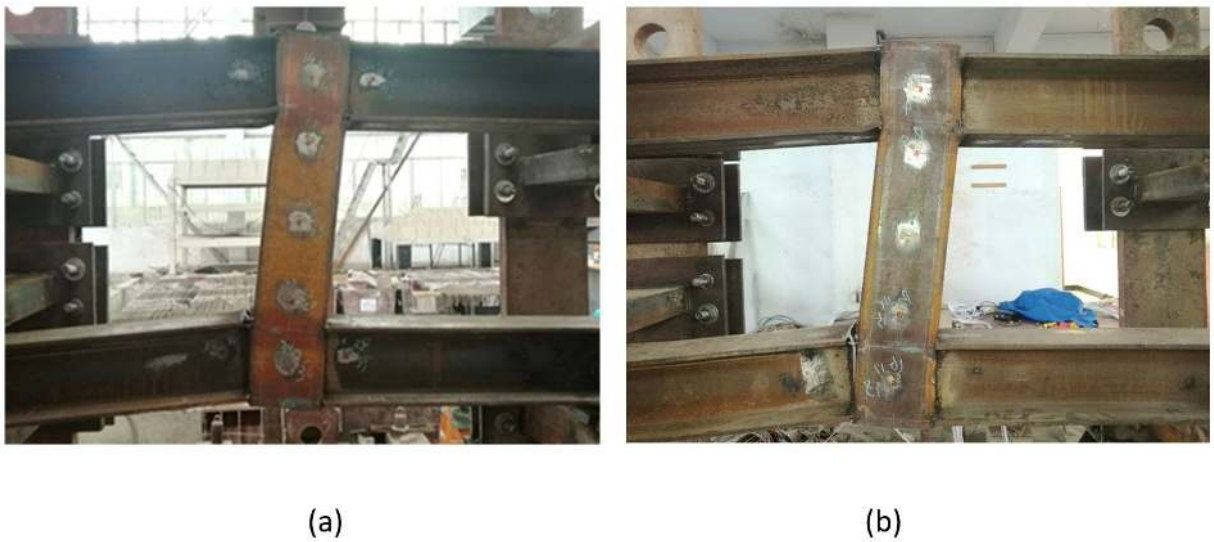

Fig.8 Integral deformation of A: (a) A-1; (b) A-2.

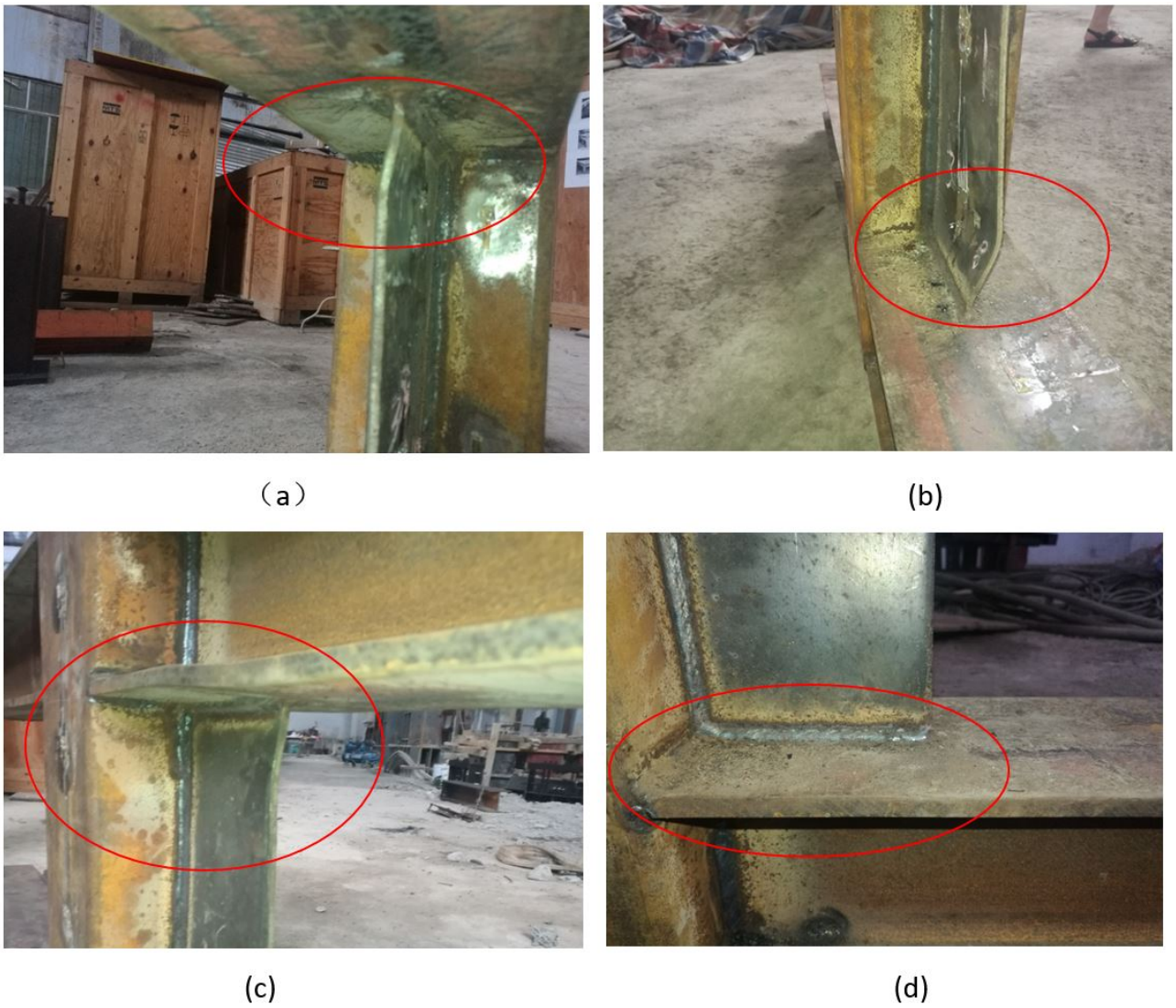

Fig.9 Detailed deformed shapes of B: (a) Deformation of the loading top; (b) Deformation of the loading bottom; (c) Deformation of the supporting top; (d) Deformation of the supporting bottom.



Fig. 10 Integral deformation of A: (a) B-1; (b) B-2.

3.2 Load-Lateral Displacement Curves

From Fig. 11, it can be seen that the load-displacement curve of A-1 specimens can be divided into two stages: elastic stage (O-E) and elastic-plastic strengthening stage (E-F). The load-displacement curve of B-2 specimens can be divided into three stages: elastic stage (O-A), elastic-plastic strengthening stage (A-B) and failure stage (B-C). From the slope of load-displacement curves, it can be seen that the lateral stiffness of Group B is significantly increased due to the action of stiffening plates. Using inflection point data to calculate the curve slope, the elastic stage slope of A-1 (O-E) is 45.63 kN/mm and B-2 (O-A) is 74.01 kN/mm, which is 62% higher than that of A-1; the elastic-plastic stage slope of A-1 (E-F) is 5.58 kN/mm and B-2 (A-B) is 15.02 kN/mm, which is 168% higher than that of A-1. It can also be seen that the bearing range of the shear key area is expanded, and the stiffness of the shear key is obviously improved due to the role of the stiffening plate.

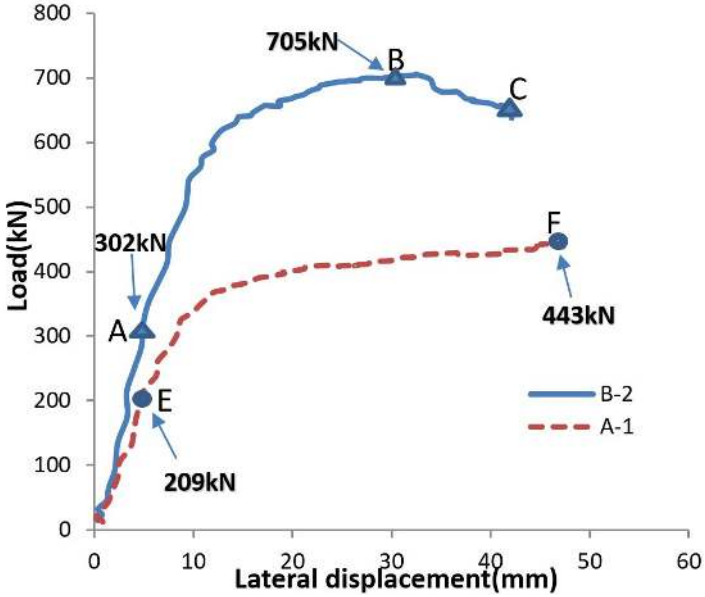

Fig.11 The loading-displacement curves of A-1 and B-2

3.3 Yield Ratio and Ductility factor

The yield ratio and the ductility factor are two critical parameters to measure the elastic-plastic performance of structures. From Table 2, it can be seen that the yield load and ultimate load of B are 1.5 times of those of A. The yield ratios of A is 2.2 and B is 2.3. The ductility factors of A and B are 10.1 and 7.5 respectively. This shows that the yield ratio of the shear key is equal while the ductility coefficient is reduced due to the setting of vertical stiffening plates, but the shear key still has good ductility deformation ability.

Table 2 Yield ratios and ductility factors of shear key

Specimen number	Yield load	Yield displacement	Ultimate load	Limit displacement	Yield ratio	Ductility factor
	F_y/kN	Δ_y/mm	F_u/kN	Δ_u/mm	F_u/F_y	Δ_u/Δ_y
A1	209	4.58	443	46.46	2.12	10.14
A2	192	4.32	449	43.7	2.34	10.12
B1	292	4.25	692	32.1	2.37	7.55
B2	302	4.08	705	30.9	2.33	7.57

3.4 Load-stress curve

The MISES stress can be calculated through the measurement of the strain flowers. The effect of vertical stiffening plate on the stress of the shear key was studied by comparing the stress of A-1 specimen and B-2 specimen at the same location. The locations of the measuring points are shown in Fig. 4 and Fig. 5. The load-stress curves of each measurement point are shown in Fig. 12. Based on the load corresponding to the yield strength of A-1 specimens, the stress of B-2 specimen is compared. The related analysis data are shown in Table 3. As it can be seen from Fig. 12 and table 3, the strain growth rate of B-2 decreases greatly due to the effect of stiffening plate. When the point stress of square steel tube of A-1 reaches to the yield strength, the corresponding point stress of B-2 is only 50%-60% of the former, and the stress level of horizontal stiffening plate of the tube is only about 30% of the former, which shows that stiffening plate plays a very good role in protecting the square steel tube. It indicates that the vertical stiffeners can greatly enhance the stiffness of the shear key and improves the bearing capacity of the specimens.

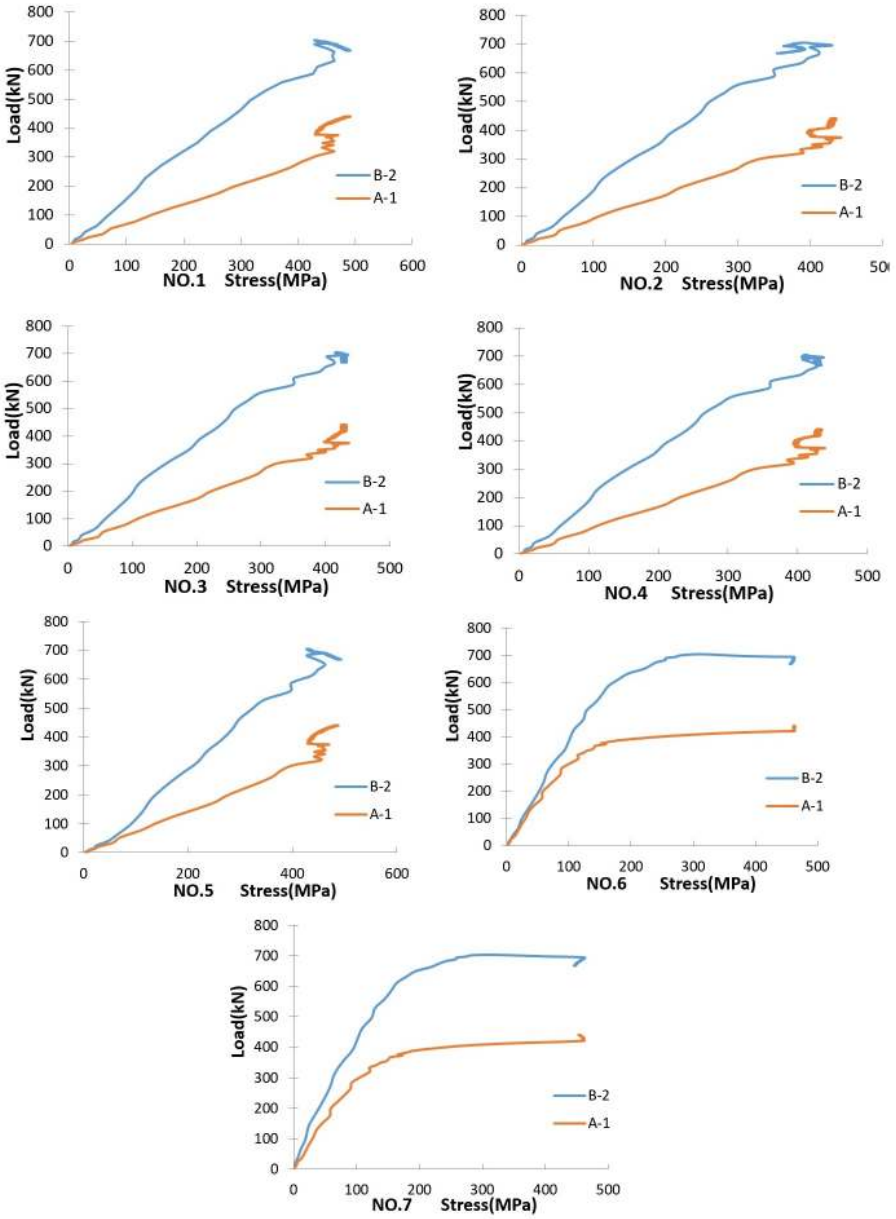

Figure 12. Load-stress curves of A-1 and B-2

Table 3 Data analysis of measuring points

Specimen number	Parameter	NO.1	NO.2	NO.3	NO.4	NO.5	NO.6	NO.7
A-1	Yield load/kN	303	407	413	416	332	420	418
	Stress/MPa	421	421	421	421	421	421	421
B-2	Load/kN	303	407	413	416	332	420	418
	Stress/MPa	206	234	254	260	222	127	130

4 Finite element analysis

4.1 Modeling parameters

ABAQUS software was used to model and analyze specimens of Groups A and B. In the finite element models, shell elements were utilized to simulate the members. The measured values were used for the geometrical dimension and material parameters of the model. The material parameters are shown in Table 1. The elastic modulus is measured in Table 1. Poisson's ratio is 0.3. Bilinear Isotropic Hardening Plasticity (BISO) is used for constitutive relationship of materials.

The boundary conditions of the model were determined according to the experiment. Linear displacements were constrained by hinged supports in three directions, and the vertical and lateral displacement were constrained by the pulley support.

4.2 Comparisons of load-displacement curves

The comparison of A-1 and B-2 between experimental and numerically simulated load-displacement curves is shown in Fig. 13. In the small deformation stage, the experimental load-displacement curves of A-1 and B-2 are in good agreement with the simulated curve, and the former is slightly smaller than the latter. With the increase of deformation, the slope of the experimental curve is larger than that of the simulated curve. The reason is that the pulley supports produces certain deformation due to the increase of the load. At the same time, the specimen itself has a larger deformation and cannot maintain the horizontal sliding, which needs to offset the force generated by the deformation. The basic trend of the experimental curve is the same as that of the simulated curve, and the finite element analysis reflects the stress law of the shear key more clearly.

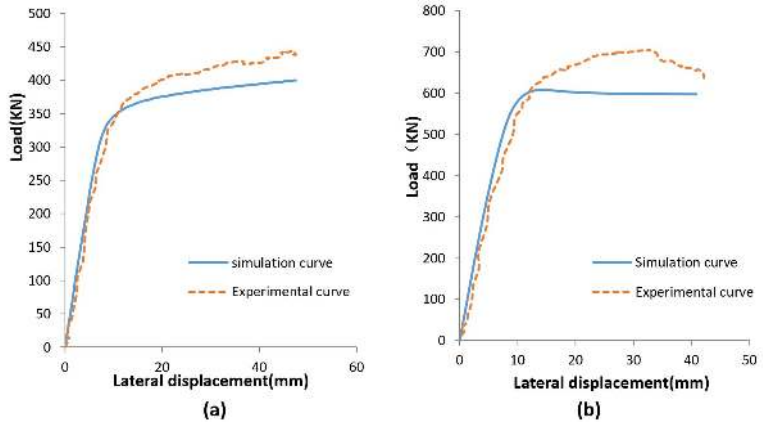

Figure 13. The comparisons of Load-Displacement Curves (a) The comparison of Load-Displacement Curve for A; (b) The comparison of Load-Displacement Curve for B.

4.3 Stress distribution analysis

At each loading stage, the MISES stress nephogram of specimen A is shown in Fig. 14. From the figure, it can be seen that in the initial stage of the loading, there is the main stress concentration area at the joint of ribs and tube, where yielding will occur first. With the increase of load, the yield range gradually diffuses to the upper and lower ends of the tubes. Under the ultimate load state, the tube is torn at the connection of rib, while the middle part of the tube is still mostly under yield stress. The tube presents Z-shaped deformation.

At each loading stage, the MISES stress nephogram of specimen B is shown in Fig. 15. From the figure, it can be seen that in the initial stage of the loading, there is the main stress concentration area at the corner of vertical stiffener, where yielding occurs first. With the increase of the load, the yielding area gradually is enlarged and diffused to the tubes. The stress is more uniform, and the deformation of the shear key is smaller.

Through the stress distributions of the specimens, it can be found that the vertical stiffening plates make the rib and square tube work together and sequently it makes the stress of the shear key more uniform. Once the volume of the shear key is increased, the bearing range of the area is enlarged which greatly improves the bearing capacity of the shear key.

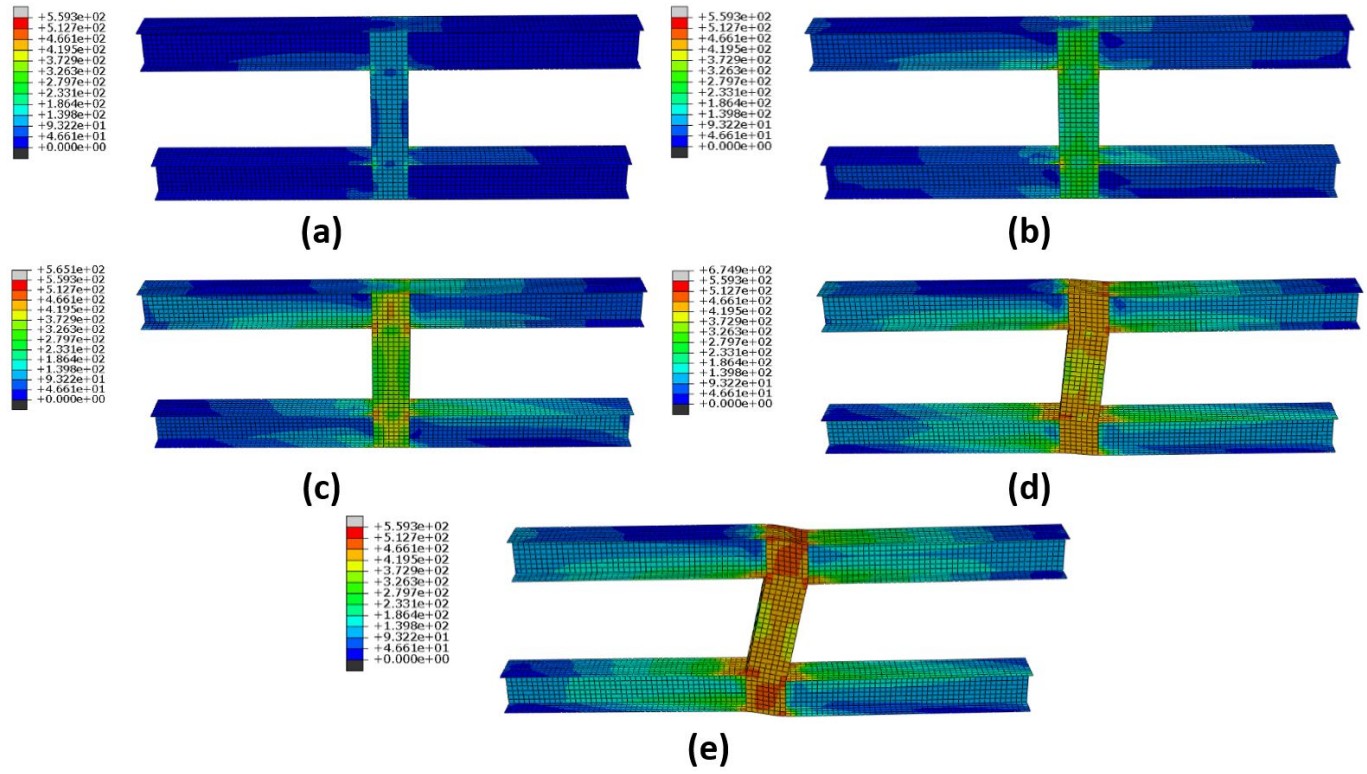

Figure 14. The MISES stress nephogram of specimen A (a)The load of 100KN; (b)The load of 200KN; (c)The load of 300KN; (d)The load of 400KN; (a)The load of 420KN;

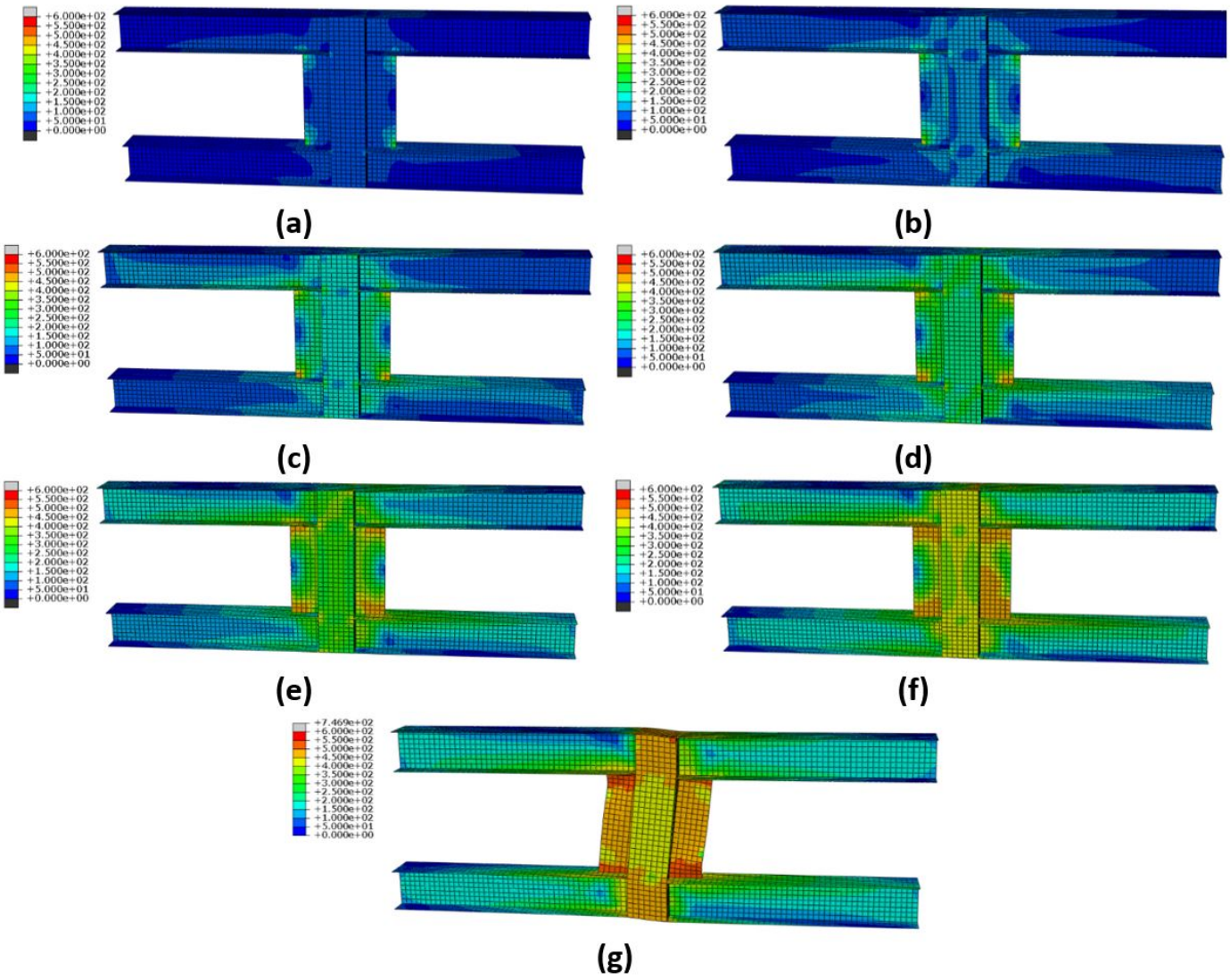

Figure 15. The MISES stress nephogram of specimen B (a)The load of 100KN; (b)The load of 200KN; (c)The load of 300KN; (d)The load of 400KN; (e)The load of 500KN; (f)The load of 600KN; (g)The load of 700KN;

5.Parametric studies of vertical stiffening plate

The setting of vertical stiffeners can significantly enhance the shear stiffness of shear key and increase the bearing capacity of specimens. The influences of the width and thickness of stiffening plate on the bearing capacity can be studied by parametric analysis method. The analysis results can determine the reasonable design parameters of stiffening plate and provide theoretical principles for similar structural design.

5.1 Parameter selection

Standard parameters are set for Specimen B. In the parametric analysis model, the other parameters are the same except for the parameter items. The data of parameter items are shown in Table 4 and Table 5.

Tab.4 Parametric analysis data of stiffener width

Parameter items	Parameter values(mm)												
Stiffener width	0	25	50	75	100	125	150	175	200	225	250	275	300

(Notes: Stiffener thickness =125mm)

Tab.5 Parametric analysis data of stiffener thickness

Parameter items	Parameter values(mm)												
Stiffener thickness	0	1	2	3	4	5	6	7	8	9	10	11	12

(Notes: Stiffener width =6mm)

5.2 Parametric analysis results

Based on parameter items, 26 parametric analysis models were built according to the parameters in Table 4 and Table 5. The loading and boundary conditions of each model are the same as those of the test. The ultimate load of each model is extracted. The curves of width-ultimate load of stiffening plate are shown in Fig. 16(a), and the curves of thickness-ultimate load are shown in Fig. 16(b). The width analysis data of stiffening plate is shown in Table 6, and the thickness analysis data is shown in Table 7.

From Fig. 16(a) and Table 6, it can be seen that the width-ultimate load curve can be divided into three stages. The inflection points of stages are 100mm, 200mm and 300mm respectively. From the analysis data in Table 6, it can be seen that when the width of stiffening plate increases from 100 mm to 200 mm, the curve slope is the largest, and the increase of bearing capacity has the maximum value. The width of stiffening plate is too small to give full play to the bearing capacity of the shear key, which causes hidden dangers to the structural safety. If the width is too large, materials would be wasted. However, this has not obvious effect on improving the performance of the specimen. As be showned in fig. 5, the width of shear key is defined as the sum of the square tube width and the stiffening plate width on both sides, the height of shear key is the clearance height between the top and bottom ribs (Shang, Ma, Dai, Liu, Zhang, 2018; Luan, 2016). In practical engineering applications, it is generally required that the height-width ratio should not be less than 1 (by welding stiffeners on both sides of the tube to meet the requirements of height-width ratio) (Shang, Ma, Dai, Liu, Lu, Li, 2018; Hu & Ma 2012). In this way, the requirements of safety and economy are satisfied.

From Fig. 16(b) and Table 7, it can be seen that the thickness-ultimate load curve of vertical stiffening plate can be divided into three stages. The inflection points of stages are 4mm, 8mm and 12mm respectively. According to the analysis data in Table 7, when the thickness increases from 4 mm to 8 mm, the curve slope is the largest, and the increase of bearing capacity reaches to the maximum value. Similarly, the thickness of stiffening plate is too small to give full play to the bearing capacity of the shear key and the stability of the stiffeners. If the thickness is too large, materials would be wasted. However, this has not obvious effect on improving the performance of the specimen. In practical engineering applications, the thickness of stiffeners can take the same as that of square.

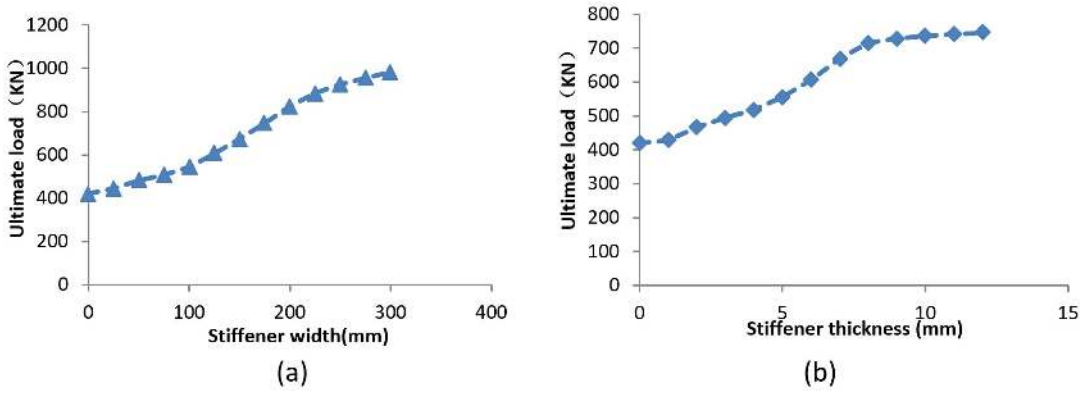

Figure 16. Parametric analysis curve (a) The curves of width-ultimate load of stiffening plate (thickness = 6mm), (b)The curves of thickness-ultimate load of stiffening plate (width = 125mm).

Table 6 Analysis data of stiffening plate width

Stiffener width	0-100mm	100mm-200mm	200mm-300mm
Ultimate load variation	419kN-545kN	545KN-824kN	824KN-981kN
Slope of curve	1.25	2.79	1.58
Ultimate load improvement	29.84%	51.18%	19.12%

Table 7 Analysis data of stiffening plate thickness

Stiffener thickness	0-4mm	4mm-8mm	8mm-12mm
Ultimate load variation	419KN-518kN	518KN-715kN	715KN-745kN
Slope of curve	24.64	49.21	7.59
Ultimate load improvement	23.47%	37.96%	4.24%

6. Conclusions

The conclusions obtained from the results of the experimental studies and the finite element analysis are as follows.

(1) Vertical stiffening plate can greatly improve the bearing capacity of the specimens.

(2) Vertical stiffening plate can make the stress of the shear key more uniform.

(3) The height-width ratio of the vertical stiffening plate should not be less than 1.

Author's Contributions: Conceptualization, H Shang and K Ma; Software, H Shang; Validation, H Shang and K Ma; Formal analysis, H Shang; Investigation, H Shang and Y Wei; Funding acquisition, Y Wei and Y Lu; Writing—original draft, H Shang; Writing—review & editing, H Shang and K Ma.

Editor: Rogério José Marczak.

REFERENCES

Da Silva, J.G.S., da S Vellasco, P.C.G., de Andrade, S.A.L., da CP Soeiro, F.J., and Werneck, R.N. (2003). An evaluation of the dynamical performance of composite slabs. Computers and Structures, 81,18-19:1905-1913.

De Silva, S.S., and Thambiratnam, D.P. (2009). Dynamic characteristics of steel-deck composite floors under human-induced loads. Computers and Structures, 87,17-18:1067-1076.

El-Dardiry, E., and Ji, T. (2005). Modelling of the dynamic behaviour of profiled composite floors. Engineering Structures, 28,4: 567-579.

Lawson, R.M., Mullett, D.L., and Rackham, J.W. (1999). Design of asymmetric slim floor beams using deep composite decking. London: The Steel Construction Institute.

Lawson, R.M., Lim, J., Hicks, S.J., and Simms, W.I. (2006). Design of composite asymmetric cellular beams and beams with large web openings. Journal of Constructional Steel Research, 62,6: 614-629.

Hicks, S. (2003). Current trend in modern floor construction. Mag Br Constr Steelwork Assoc (BCSA), 11, 1:32-3.

Shang, H., Ma, K., Wei. Y., Dai. Z., Liu, J. (2018). Structural design of large-span monolithic precast H-shape steel spatial grid plate. Building Structure, 48,7:9-13.

Ma, K., Zhang, H., Zheng, T. (2006). Theory and Practice of New Type Architectural Space Griding structures. Beijing: China Communications Press.

Shang, H., Ma, K., Dai, Z., Liu, J., Zhang, H. (2018a). Anti-explosion design and dynamic analysis on assembled monolithic orthogonal-diagonal lattice H shape steel spatial grid roof. Industrial Construction, 48,4:130-136.

Shang, H., Ma, K., Dai, Z., Liu, J., Lu, Y., Li, L. (2018b). Vibration study and parametric analysis on assembled monolithic orthogonal H shape steel spatial grid plate under human-induced loads. Spatial Structures, 24,3:32-40.

Zhang, H., Ma, K. (2003). Simplified Algorithm for Analysis of Stiffness and Static Behavior of Reinforced Concrete Vierendeel Sandwich Plate. Journal of Guizhou University of Technology (Natural Edition), 32,5:66-71.

Zhang, H., Ma, K., Zheng, T., Hu, H. (2004). Continuum analysis method for cast-in-place reinforced concrete hollow plate. Spatial Structures, 10,4:12-15.

Zhang, Y. (2010). Calculation of natural frequencies of shear keys dowelled open web sandwich plates under different boundary conditions. Spatial Structures, 16,1:35-38.

Jiang, L., Zhang, H. (2014). Dynamic analysis of large span open-web sandwich plate based on comfort requirement. Spatial Structures, 20,3:56-60.

Bai, Z., Ma, K., Sun, T., Lu, Y. (2016). Study of fundamental frequency of reinforced concrete open-web sandwich plates. Industrial Construction, 46,7:108-113.

Cai, Q., Ma, K., Shen, B.(2017).Natural frequency analysis of the honeycomb type steel open-web sandwich plate floor based on vibrate comfort requirement. Building Science,33,5:1-7.

Technical code of cold-formed thin-wall steel structures. (2002). In GB 50018-2002, Beijing: China Planning Press.

Metallic materials-Tensile testing at ambient temperature. (2010). In GB/T 228.1-2010, Beijing: Standards press of china.

Luan, H. (2016). Investigation on structural behavior of an innovative orthogonal-diagonal steel open-web floor system. Advances in Structural Engineering, 19,2:353-371.

Hu, L., and Ma, K. (2012). Research and application of U-shaped steel plate-concrete composite open-web slab structure with high strength bolts. Journal of Building Structures, 33,7: 61-69.